Received 10 August; accepted 15 October 2003; doi:10.1038/nature02123.
Published online 16 November 2003.

1. Denli, A. M. & Hannon, G. J. RNAi: an ever-growing puzzle. *Trends Biochem. Sci.* **28,** 196–201 (2003).
2. Hutvagner, G. & Zamore, P. D. RNAi: nature abhors a double-strand. *Curr. Opin. Genet. Dev.* **12,** 225–232 (2002).
3. Hammond, S. M., Bernstein, E., Beach, D. & Hannon, G. J. An RNA-directed nuclease mediates post-transcriptional gene silencing in *Drosophila* cells. *Nature* **404,** 293–296 (2000).
4. Zamore, P. D., Tuschl, T., Sharp, P. A. & Bartel, D. P. RNAi: double-stranded RNA directs the ATP-dependent cleavage of mRNA at 21 to 23 nucleotide intervals. *Cell* **101,** 25–33 (2000).
5. Bernstein, E., Caudy, A. A., Hammond, S. M. & Hannon, G. J. Role for a bidentate ribonuclease in the initiation step of RNA interference. *Nature* **409,** 363–366 (2001).
6. Elbashir, S. M., Lendeckel, W. & Tuschl, T. RNA interference is mediated by 21- and 22-nucleotide RNAs. *Genes Dev.* **15,** 188–200 (2001).
7. Nykanen, A., Haley, B. & Zamore, P. D. ATP requirements and small interfering RNA structure in the RNA interference pathway. *Cell* **107,** 309–321 (2001).
8. Hammond, S. M., Boettcher, S., Caudy, A. A., Kobayashi, R. & Hannon, G. J. Argonaute2, a link between genetic and biochemical analyses of RNAi. *Science* **293,** 1146–1150 (2001).
9. Martinez, J., Patkaniowska, A., Urlaub, H., Luhrmann, R. & Tuschl, T. Single-stranded antisense siRNAs guide target RNA cleavage in RNAi. *Cell* **110,** 563–574 (2002).
10. Cerutti, L., Mian, N. & Bateman, A. Domains in gene silencing and cell differentiation proteins: the novel PAZ domain and redefinition of the Piwi domain. *Trends Biochem. Sci.* **25,** 481–482 (2000).
11. Kataoka, Y., Takeichi, M. & Uemura, T. Developmental roles and molecular characterization of a *Drosophila* homologue of *Arabidopsis* Argonaute1, the founder of a novel gene superfamily. *Genes Cells* **6,** 313–325 (2001).
12. Carmell, M. A., Xuan, Z., Zhang, M. Q. & Hannon, G. J. The Argonaute family: tentacles that reach into RNAi, developmental control, stem cell maintenance, and tumorigenesis. *Genes Dev.* **16,** 2733–2742 (2002).
13. Tabara, H. *et al.* The rde-1 gene, RNA interference, and transposon silencing in *C. elegans*. *Cell* **99,** 123–132 (1999).
14. Theobald, D. L., Mitton-Fry, R. M. & Wuttke, D. S. Nucleic acid recognition by OB-fold proteins. *Annu. Rev. Biophys. Biomol. Struct.* **32,** 115–133 (2003).
15. Volpe, T. A. *et al.* Regulation of heterochromatic silencing and histone H3 lysine-9 methylation by RNAi. *Science* **297,** 1833–1837 (2002).
16. Yan, K. S. *et al.* Structure and conserved RNA binding of the PAZ domain. *Nature* advance online publication, 16 November 2003 (doi:10.1038/nature02129).
17. Zhang, H., Kolb, F. A., Brondani, V., Billy, E. & Filipowicz, W. Human Dicer preferentially cleaves dsRNAs at their termini without a requirement for ATP. *EMBO J.* **21,** 5875–5885 (2002).
18. Elbashir, S. M., Martinez, J., Patkaniowska, A., Lendeckel, W. & Tuschl, T. Functional anatomy of siRNAs for mediating efficient RNAi in *Drosophila melanogaster* embryo lysate. *EMBO J.* **20,** 6877–6888 (2001).
19. Delaglio, F. *et al.* NMRPipe: a multidimensional spectral processing system based on UNIX Pipes. *J. Biomol. NMR* **6,** 277–293 (1995).
20. Johnson, B. A. & Blevins, R. A. NMRView: A computer program for the visualization and analysis of NMR data. *J. Biomol. NMR* **4,** 603–614 (1994).
21. Sattler, M., Schleucher, J. & Griesinger, C. Heteronuclear multidimensional NMR experiments for the structure determination of proteins in solution employing pulsed field gradients. *Prog. NMR Spectrosc.* **34,** 93–158 (1999).
22. Cornilescu, G., Delaglio, F. & Bax, A. Protein backbone angle restraints from searching a database for chemical shift and sequence homology. *J. Biomol. NMR* **13,** 289–302 (1999).
23. Linge, J. P., O'Donoghue, S. I. & Nilges, M. Automated assignment of ambiguous nuclear overhauser effects with ARIA. *Methods Enzymol.* **339,** 71–90 (2001).
24. Brünger, A. T. *et al.* Crystallography & NMR system: A new software suite for macromolecular structure determination. *Acta Crystallogr. D* **54,** 905–921 (1998).
25. Linge, J. P., Williams, M. A., Spronk, C. A., Bonvin, A. M. & Nilges, M. Refinement of protein structures in explicit solvent. *Proteins* **50,** 496–506 (2003).
26. Laskowski, R. A., Rullmannn, J. A., MacArthur, M. W., Kaptein, R. & Thornton, J. M. AQUA ROCHECK-NMR: programs for checking the quality of protein structures solved by NMR. *J. Biomol. NMR* **8,** 477–486 (1996).
27. Koradi, R., Billeter, M. & Wüthrich, K. MOLMOL: a program for display and analysis of macromolecular structures. *J. Mol. Graph.* **14,** 51–55 (1996).
28. Nicholls, A., Sharp, K. A. & Honig, B. Protein folding and association: insights from the interfacial and thermodynamic properties of hydrocarbons. *Protein Struct. Funct. Genet.* **11,** 281–296 (1991).
29. Grüter, P. *et al.* TAP, the human homolog of Mex67p, mediates CTE-dependent RNA export from the nucleus. *Mol. Cell* **1,** 649–659 (1998).
30. Bogden, C. E., Fass, D., Bergman, N., Nichols, M. D. & Berger, J. M. The structural basis for terminator recognition by the Rho transcription termination factor. *Mol. Cell* **3,** 487–493 (1999).

Supplementary Information accompanies the paper on **www.nature.com/nature**.

Acknowledgements We thank A. Ladurner, E. Conti and R. Russell for discussions; G. Stier and S. Bäckström for the pETM60 vector; M. Rode for technical support; F. Ciccarreli and P. Bork for help with sequence alignments; and the NMR centre in Frankfurt, Germany for NMR measurement time. This study was supported by the European Molecular Biology Organization (EMBO), the German Research Foundation (DFG), and the Human Frontier Science Program Organization.

Competing interests statement The authors declare that they have no competing financial interests.

Correspondence and requests for materials should be addressed to E.I. (izaurralde@embl.de) or M.S. (sattler@embl.de). The coordinates and NMR data of the Ago2 PAZ domain have been deposited in the Protein Data Bank under accession number 1upo.

Structure and conserved RNA binding of the PAZ domain

Kelley S. Yan, Sherry Yan, Amjad Farooq, Arnold Han, Lei Zeng & Ming-Ming Zhou

Structural Biology Program, Department of Physiology and Biophysics, Mount Sinai School of Medicine, New York University, One Gustave L. Levy Place, New York, New York 10029-6574, USA

The discovery of RNA-mediated gene-silencing pathways, including RNA interference[1–3], highlights a fundamental role of short RNAs in eukaryotic gene regulation[4–10] and antiviral defence[11,12]. Members of the Dicer and Argonaute protein families are essential components of these RNA-silencing pathways[13–19]. Notably, these two families possess an evolutionarily conserved PAZ (Piwi/Argonaute/Zwille) domain whose biochemical function is unknown. Here we report the nuclear magnetic resonance solution structure of the PAZ domain from *Drosophila melanogaster* Argonaute 1 (Ago1). The structure consists of a left-handed, six-stranded β-barrel capped at one end by two α-helices and wrapped on one side by a distinctive appendage, which comprises a long β-hairpin and a short α-helix. Using structural and biochemical analyses, we demonstrate that the PAZ domain binds a 5-nucleotide RNA with 1:1 stoichiometry. We map the RNA-binding surface to the open face of the β-barrel, which contains amino acids conserved within the PAZ domain family, and we define the 5′-to-3′ orientation of single-stranded RNA bound within that site. Furthermore, we show that PAZ domains from different human Argonaute proteins also bind RNA, establishing a conserved function for this domain.

The three-dimensional structure of the minimal PAZ domain of *D. melanogaster* Ago1 (residues 298–427) is well defined by nuclear magnetic resonance (NMR) (Fig. 1a; see also Supplementary Table 1). Its compact architecture is built on a left-handed, six-stranded β-barrel core consisting of amino acid sequences conserved within the PAZ domain family[20] (Fig. 1b, c; see also Supplementary Fig. 1). Helices α1 and α2 pack together to close off one end of the barrel by forming interactions between Val 305, Met 309 and Phe 333, and the hydrophobic core of the barrel. A long β-hairpin (β5–β6) and a short helix α3 form a structural appendage that is inserted between β4 and β7, and wraps around the rim of the β-barrel along β8 (Fig. 1b, c). Although this appendage is an integral part of the PAZ domain structure, residues in β5 and β6 exhibit high dynamics (Supplementary Fig. 2). These structural elements are tied together by the amino- and carboxy-terminal regions that form a small anti-parallel β-sheet (β1 and β10), emphasizing the modular nature of this domain. Notably, although the conserved C-terminal residues 430–464 (Supplementary Fig. 1) are predicted to be a long α-helix, our NOE (nuclear Overhauser effects) analysis shows that they are unstructured (Supplementary Fig. 2). Truncation of this C-terminal segment did not affect the structure, confirming that it is not essential for the isolated PAZ domain.

Sequence conservation implies that the β-barrel also serves as the structural core for other Argonaute family PAZ domains, and the appendage may also be present with a β-hairpin of variable length (Supplementary Fig. 1). Significant variations exist in the loop sequences of different PAZ domains, possibly reflecting differences in cellular function. Dicer PAZ domains exhibit major sequence deviations from the Argonaute PAZ domains in the β7–β8 loop, although they probably still adopt the basic β-barrel and α3 structure. The *D. melanogaster* Ago1 PAZ domain has a highly positive electrostatic potential (Fig. 1d), but most of its Arg and Lys residues are not conserved in other PAZ domains. Highly conserved residues including Tyr 354, Pro 363 and Tyr 386 are clustered at the

entrance of the β-barrel (Figs 1c and 3a; see also Supplementary Fig. 1), suggesting a possible functional site. Owing to the high level of structural conservation, we define the β-barrel and its associated appendage as the PAZ fold.

Despite its suggested function in protein–protein interaction[17], the β-barrel core of the PAZ fold topologically resembles that of the RNA-binding domain of Sm proteins[21] (Supplementary Fig. 3). We explored the possibility of nucleic-acid binding using NMR titration, and found that the Ago1 PAZ domain binds single-stranded (ss)RNA oligonucleotides with high preference over ssDNA counterparts (Fig. 2a). As demonstrated in two-dimensional ^{1}H-^{15}N-HSQC (heteronuclear single quantum coherence) spectra (Fig. 2b), the protein forms a 1:1 stoichiometric complex with a 5′-pUGACA ssRNA (dissociation constant (K_d) approximately 1 μM), a consensus sequence found at the 5′ ends of microRNAs (miRNAs)[22]. The PAZ domain binds this ssRNA marginally better than the corresponding double-stranded (ds)RNA, and this interaction does not require the unstructured C-terminal segment (data not shown). Moreover, the RNA binding appears independent of sequence, as the protein binds equally well to different RNAs including a 5′-pUGAGG derived from the 5′ end of *let-7* miRNA[23]. The length of RNA does affect binding. Addition of ssRNA longer than 9–11 bases, or of prototypical 21-nt siRNA duplexes with 5′ phosphates and 2-nt 3′ overhangs, results in severe line broadening of NMR signals for the vast majority of the PAZ domain residues that is reversible with RNase treatment (data not shown). This line-broadening phenomenon may be explained by: multiple PAZ domain molecules binding to a single RNA molecule, forming a complex analogous to 'protein beads on an RNA string'; or by a single PAZ domain engaging in different modes of interactions with a single RNA molecule (that is, 'sliding' through the RNA sequence), resulting in coexistence of different complex species. Both possibilities are consistent with the sequence-independent RNA binding of the PAZ domain.

Short regulatory RNAs have characteristic 5′ phosphate and 3′ hydroxyl groups, and 5′ phosphorylation is required for incorporation into the RNA-induced silencing complex (RISC) in RNA interference[24–27]. Indeed, comparison of the binding of the Ago1 PAZ domain to 5′-pUGACA and 5′-UGACA revealed that although the two ssRNAs use the same mode of interaction, as assessed by the similar pattern of chemical shift perturbations, the 5′ phosphorylated RNA results in additional resonance changes and reduced line broadening for a subset of protein residues (Fig. 2c), possibly indicative of higher affinity binding. Modification of the 5′ phosphate group by an amino-methylene (3-carbon) linkage[27] reduces the binding affinity (K_d approximately 2 μM). These observations suggest that 5′ phosphorylation may contribute to the PAZ domain–RNA interaction. Preliminary data using a 5′ phosphorylated ssRNA with a 3′-biotin modification showed that immobilized protein failed to pull down purified Ago2 PAZ domain (data not shown). By NMR titration, this substrate had a reduced binding affinity (K_d greater than 20 μM), suggesting that the 3′ end may also

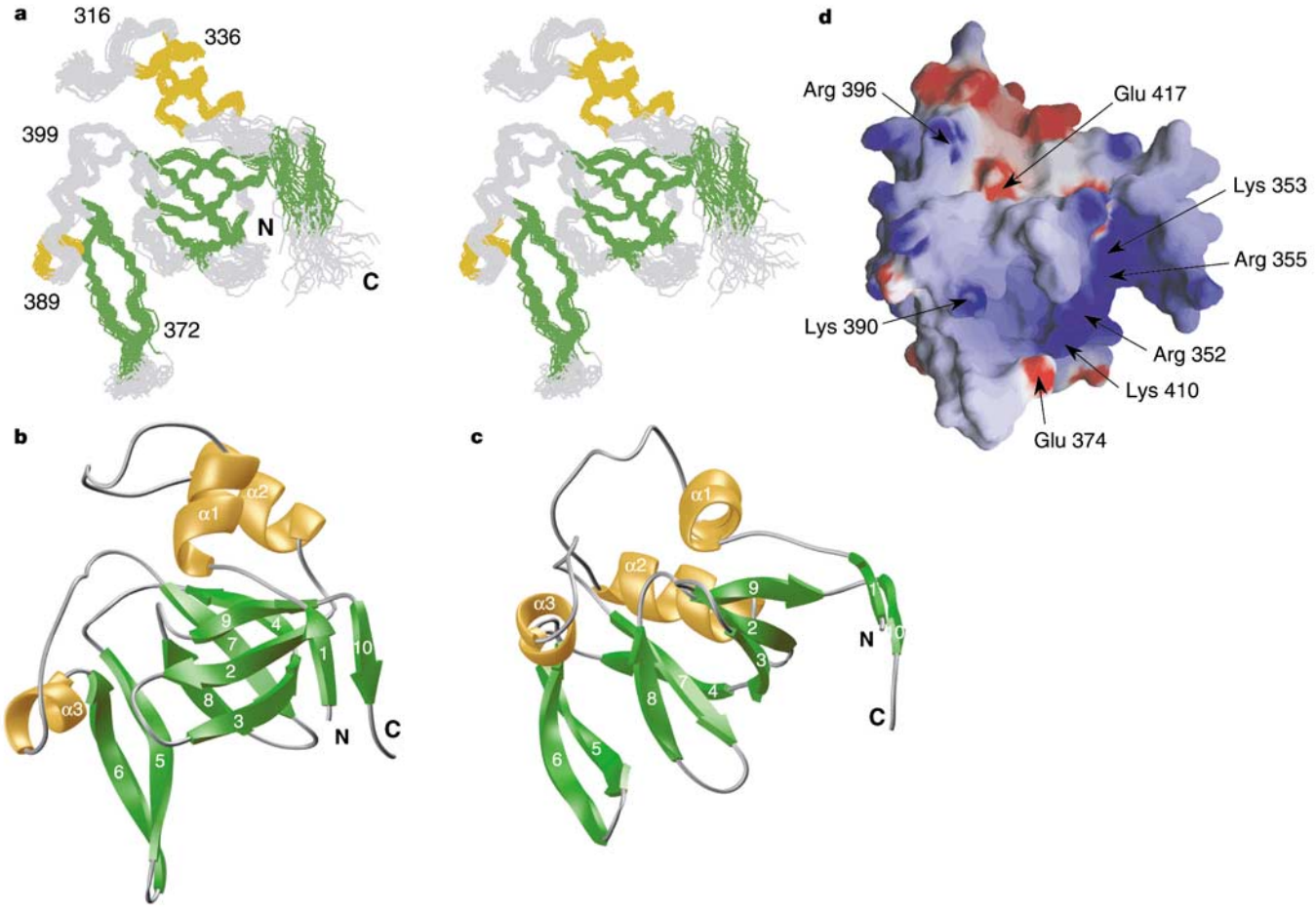

Figure 1 Three-dimensional structure of the *D. melanogaster* Ago1 PAZ domain. **a**, Stereoview of the backbone atoms of 25 superimposed NMR-derived structures of the PAZ domain (residues 298–430). The C-terminal unstructured residues (431–464) are omitted for clarity. **b**, Ribbons depiction (side view) of a representative NMR structure. The orientation of **b** is similar to that in **a**. **c**, Top view of the PAZ domain. **d**, The surface electrostatic potential (blue, positive; red, negative) of the PAZ domain calculated in GRASP, displayed in the some orientation as **c**.

play a role in PAZ domain interaction.

We further characterized the Ago1 PAZ domain–RNA interaction with an RNA electrophoretic mobility shift assay (EMSA). However, possibly due to Ago1's high isoelectric point of 9.5 and the nature of RNA interactions, the ribonucleoprotein complex was not directly detected by EMSA. As shown in the NMR study, this PAZ domain can form a 1:1 stoichiometric complex with short RNA (about 5–7 nucleotides), or a 'protein beads on an RNA string' complex with longer RNA. In both cases, the complex is too positively charged at pH 8.3 to migrate towards the positive electrode in an EMSA. This reasoning seems consistent with the observation of a stable protein–RNA complex in an EMSA with human Piwi-like 1 PAZ domain (pI of 7.0; see below). Alternatively, this lack of detection of the *D. melanogaster* Ago1 PAZ domain–RNA complex might be due to the kinetic instability of the complex. However, we observed that the free ^{32}P-labelled RNA band decreases as a function of increasing Ago1 PAZ domain concentration (Fig. 2d), indicating formation of a protein–RNA complex. This RNA binding could be effectively competed away by unlabelled RNA of identical sequence, but to a lesser extent by DNA (Fig. 2d). These data confirm that the *D. melanogaster* Ago1 PAZ domain is able to interact with RNA preferentially over DNA.

The PAZ domain residues that undergo chemical shift changes upon RNA binding are localized at the open end of the β-barrel and the appendage, which together form an elongated binding groove (Fig. 3a, b). This cleft contains many of the residues highly conserved among PAZ domains. Because the PAZ domain binds 5′ phosphorylated and 5′ hydroxyl ssRNA in a similar manner, differential chemical shift perturbation analysis enabled us to define the 5′-to-3′ orientation of the ssRNA bound within this groove (Fig. 2c). Out of a small number of residues, Gln 407 and Arg 355 showed the most profound differences in chemical shift perturbations, suggesting that the 5′ end of a ssRNA molecule binds to a site in the region of the β3–β4 loop and the end of β7. The 3′ end binding site possibly involves an aromatic cluster at α3 containing the conserved Tyr 386, Phe 387 and Tyr 391 residues. End to end, the RNA-binding groove spans approximately 35–40 Å in length, corresponding to the length of a 5–7-nucleotide RNA that forms a stable 1:1 complex with the PAZ domain.

Using NMR, we probed the molecular nature of PAZ domain–RNA interactions with UMP (uridine 5′-monophosphate). Despite its low affinity (K_d approximately 2 mM), UMP is bound in the predicted RNA-binding groove, as revealed by the structure of the PAZ domain–UMP complex (Fig. 3c, d). The 2′ and 3′ hydroxyl groups are positioned to form hydrogen bonds with the backbone atoms of His 411 and Thr 412 of β8 (Fig. 3d). The aromatic uracil interacts with the terminal nitrogen of Lys 410, and the 5′ phosphate of UMP is possibly coordinated by the nitrogen atoms of Arg 352. The intermolecular NOEs to the ribose are greater in number (11 compared with 2) and intensity than those seen to the base, indicating that recognition of UMP involves mostly the sugar moiety rather than the base. These observations agree with our finding of the PAZ domain preference of RNA over DNA and the apparent lack of sequence dependence. As the intermolecular NOEs observed for ssRNA also involve the same set of residues conserved in sequence, the PAZ domain–UMP complex structure provides valuable insights into RNA recognition.

To investigate the molecular determinants of RNA binding by the Ago1 PAZ domain, we performed site-directed mutagenesis on 15 amino acid residues that are localized to the RNA-binding groove and conserved in the PAZ domain family. The effect of these mutations on RNA binding was assessed by the ability of the mutants to compete with wild-type PAZ domain for binding to ssRNA (Fig. 3e; see also Supplementary Fig. 4). Individual mutation of Tyr 354, Met 366, Lys 390, Arg 392, Arg 396 or Glu 417 to Ala did not cause major reductions in RNA binding. However, point mutation of His 346, Arg 352, Phe 369, Lys 385, Tyr 386, Phe 387, Tyr 391 or Lys 410 to Ala resulted in a greater than 50% loss of RNA binding as compared with the wild type. Notably, R355A lost nearly 90% of the RNA-binding activity. The functionally important residues as defined by mutagenesis are clustered in three regions of the PAZ fold (Fig. 3a, e): (1) the β3–β4 loop (Arg 355), a binding site for the 5′ end of ssRNA; (2) the rim of the β-barrel orifice formed by the β2–β3 and β7–β8 loops (His 346, Arg 352 and Lys 410), where UMP binds; and (3) the solvent-exposed basic and

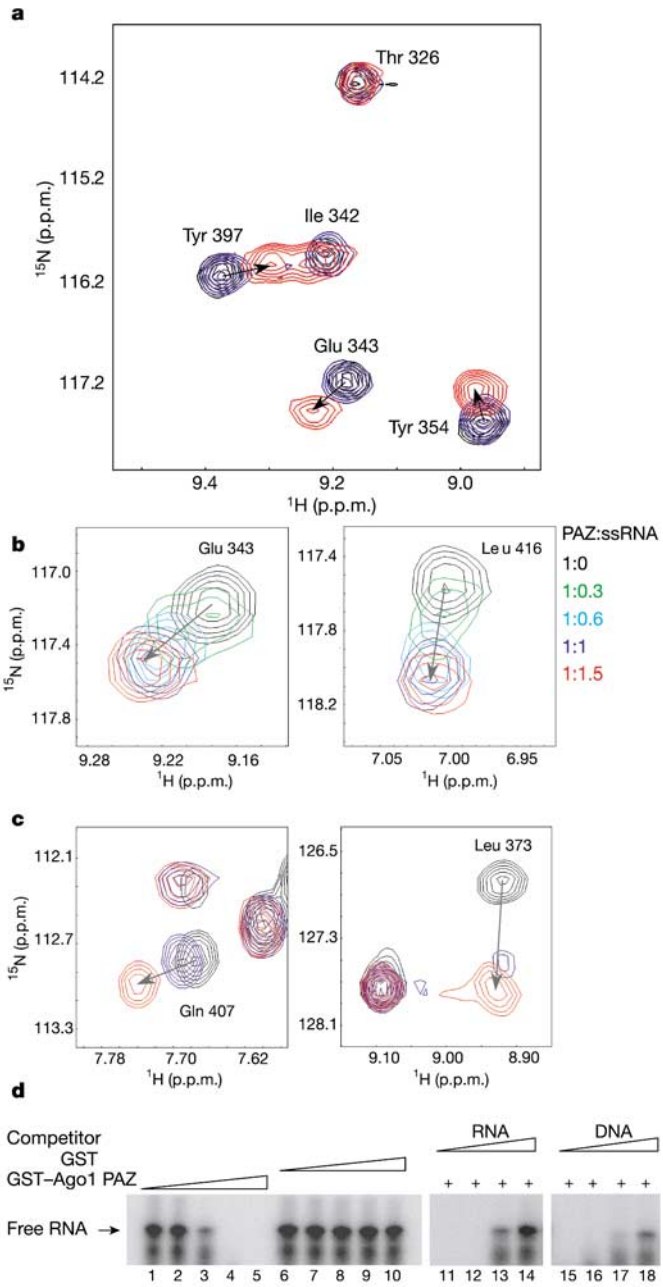

Figure 2 RNA binding of the *D. melanogaster* Ago1 PAZ domain. **a**, Superimposition of ^{1}H-^{15}N-HSQC spectra of the PAZ domain (approximately 0.3 mM) in free form (black), with 5′ phosphorylated ssDNA (5′-pTGACA; PAZ:ligand molar ratio 1:1.5) (blue) or 5′ phosphorylated ssRNA (5′-pUGACA; 1:1.5) (red). p.p.m., parts per million. **b**, Stoichiometry of PAZ domain–ssRNA binding. The amide signals of Glu 343 and Leu 416 in the superimposed NMR spectra are colour-coded according to PAZ:RNA molar ratio. **c**, Binding of 5′ hydroxyl (blue) compared with 5′ phosphorylated (red) ssRNA (UGACA). The PAZ:ssRNA molar ratio was 1:1.5. **d**, RNA electrophoretic mobility shift assay, assessing the Ago1 PAZ domain interaction with RNA and DNA.

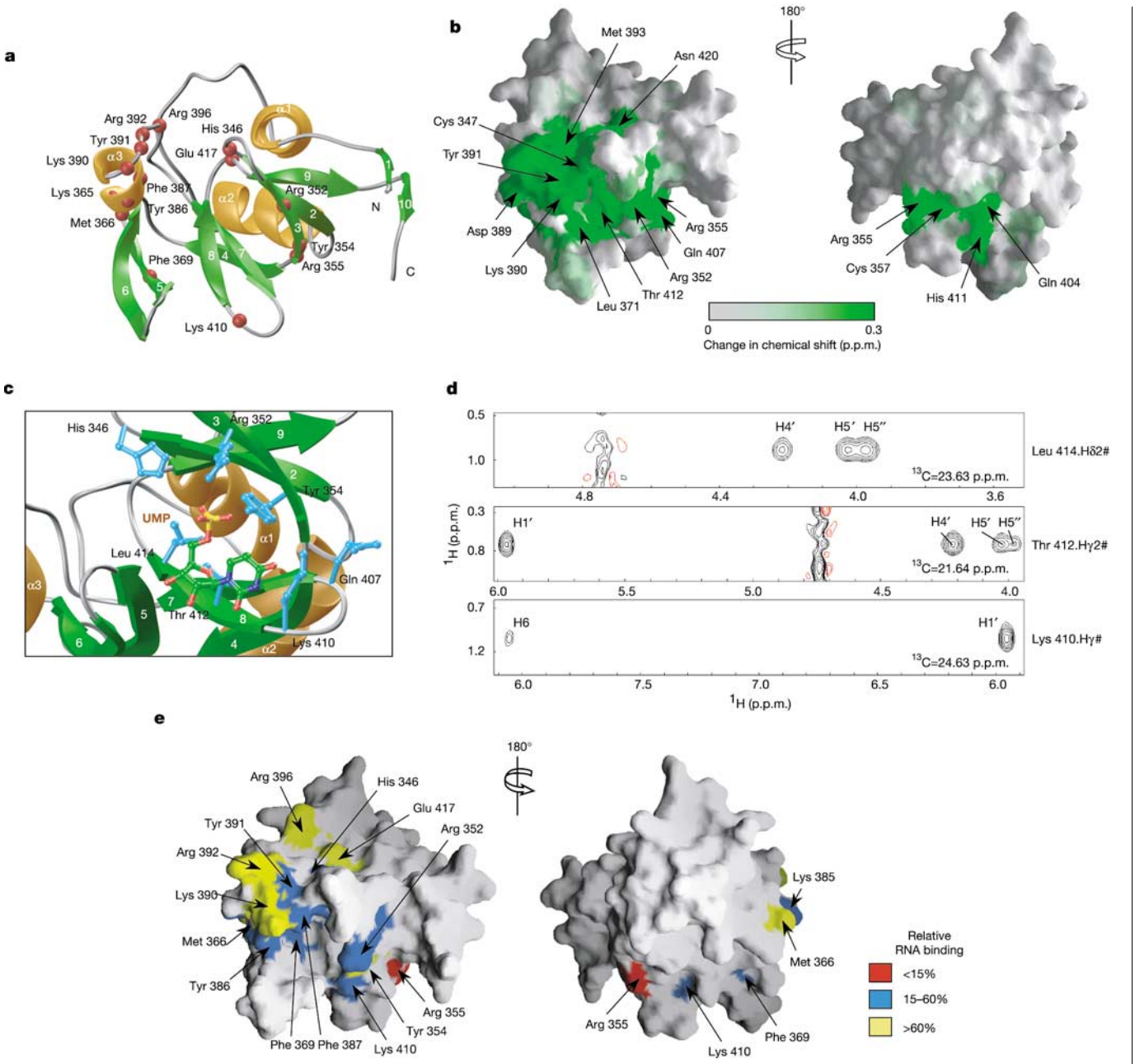

Figure 3 Mapping the RNA-binding site of the *D. melanogaster* Ago1 PAZ domain. **a**, Structure of the PAZ domain depicting residues (red spheres) conserved in the PAZ domain family. **b**, Molecular surface of the protein highlighting residues that exhibit backbone ^{1}H and ^{15}N chemical shift perturbations on binding to ssRNA (5′-pUGACA; PAZ:RNA 1:1.5). The orientation of the left panel is same as **a**. **c**, UMP binding site of the PAZ domain–UMP complex structure. **d**, Intermolecular NOEs between the PAZ domain and UMP observed in a three-dimensional ^{13}C-edited, ^{13}C/^{15}N-filtered NOESY spectrum. Hδ2#, Hγ2# and Hγ# represent specific side-chain hydrogen atoms in amino acid residues. **e**, Mutational analysis of the PAZ domain. Effects of individual mutations on RNA binding were assessed by an inhibition experiment described in the Methods and Supplementary Fig. 2, and colour-coded according to their relative RNA-binding activities. Results were normalized to 100% RNA-binding activity with the wild-type protein.

aromatic cluster at α3 (Lys 385, Tyr 386, Phe 387 and Tyr 391). The large number and extended distribution of possible contact points between the PAZ domain and RNA may explain the lack of a null point mutant, and confirm our findings on the location and geometry of the RNA-binding site in the PAZ fold.

To test whether RNA binding is a general function of the PAZ domain, we prepared PAZ domains from different subgroups of proteins within the large PAZ domain family. As predicted, the PAZ domains from human Ago1 (eIF2C1), Ago2 (eIF2C2) and Piwi-like 1 bind to ssRNA (Fig. 4a–c). Similar to *D. melanogaster* Ago1, the human PAZ domains bind RNA preferentially over DNA, and form a 1:1 stoichiometric complex with 5-nucleotide ssRNA. Moreover, the Piwi-like 1 PAZ domain–RNA complex was directly detected by EMSA (Fig. 4d). The band corresponding to the complex increases as a function of protein concentration, whereas the free RNA signal decreases accordingly. The Piwi-like 1 PAZ domain–RNA complex was effectively competed away with unlabelled RNA, but not as well with the corresponding DNA (Fig. 4d). From these results, we conclude that RNA binding is a conserved function of the PAZ domain.

The structure and RNA binding of the *D. melanogaster* Ago2 PAZ domain reported in the accompanying paper[28] are consistent with

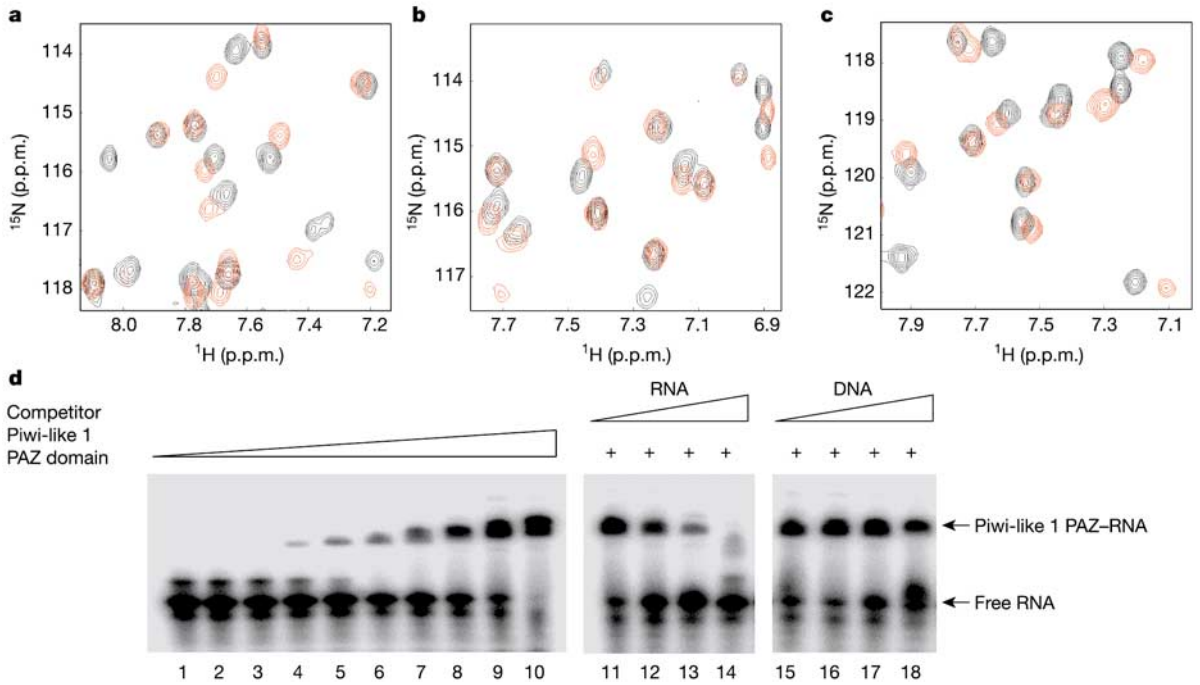

Figure 4 Conserved RNA binding of the PAZ domain. **a**–**c**, Superimposition of ^{1}H-^{15}N-HSQC spectra of the PAZ domains from human Ago1 (**a**), Ago2 (**b**) and Piwi-like 1 (**c**) in free form (black) and with a 5′-pUGAGG ssRNA (red, PAZ:RNA 1:1). **d**, RNA electrophoretic mobility shift assay assessing RNA binding of human Piwi-like 1 PAZ domain.

the predictions from our study that the PAZ fold and RNA binding are conserved in the PAZ domain family. The molecular nature and specificity of DNA binding shown by the *D. melanogaster* Ago2 PAZ domain, which is in contrast to the preference of RNA over DNA binding by the Ago1 PAZ domain demonstrated in our study, however, remains to be evaluated for its possible biological importance.

Our structure, mutagenesis and RNA mobility shift data of the PAZ domain define this module as an RNA-binding domain, thereby establishing the molecular function of this family. The PAZ domain uses a six-stranded β-barrel, similar to Sm proteins[21] but with an additional appendage, to bind both single- and double-stranded RNA. Although RNA binding by the PAZ domain *in vitro* does not appear to be sequence-dependent, *in vivo* specificity may be conferred within the context of the full-length protein or through accessory proteins within RISC. The unique features of short regulatory RNAs, such as their length of approximately 22 nucleotides and 5′ phosphate and 3′ hydroxyl ends may contribute to specificity[13,24–27]. Our data show that these 5′ and 3′ ends may enhance RNA binding by the PAZ domain, and that the binding groove accommodates RNA of 5–7 nucleotides in length. These findings may correlate with the 5′ phosphorylation requirement of siRNAs or miRNAs for their incorporation into RISC[24,27], as well as the observed length of the 5′ end sequence conservation in miRNAs[22,29]. □

Methods

Sample preparation

The PAZ domain of *Drosophila* Argonaute 1 (residues 297–464 or 297–433) was cloned into a pET19b vector and expressed in *Escherichia coli* BL21(DE3) cells as an N-terminal His_{10}-tagged protein. Uniformly ^{15}N- and ^{15}N/^{13}C-labelled proteins were prepared by growing bacteria in minimal medium with $^{15}NH_4Cl$ and/or $^{13}C_6$-glucose as the sole nitrogen and carbon sources. Deuterated protein was generated by cell growth in 95% $^{2}H_2O$. The PAZ domain was purified by nickel-NTA affinity chromatography. After cleavage of the His_{10} tag, the protein was further purified by ion-exchange and size-exclusion chromatography. Protein NMR samples (approximately 0.5 mM) were prepared in 100 mM phosphate buffer of pH 6.5, 150 mM NaCl and 5 mM dithiothreitol (DTT)-d_{10} in $H_2O/^{2}H_2O$ (9/1) or $^{2}H_2O$. PAZ domains from the human proteins Ago1 (residues 218–356), Ago2 (residues 220–358) and Piwi-like 1 (residues 604–910) were cloned into the pET19b expression vector. These proteins were expressed and purified using a procedure similar to that of the *D. melanogaster* Ago1 PAZ domain. Glutathione *S*-transferase (GST)–Ago1 PAZ domain fusion proteins were expressed in bacteria using the pGEX-6P-1 vector, and purified by affinity chromatography.

NMR spectroscopy

The Ago1 PAZ domain containing residues 297–464 was used for structure determination. All NMR spectra were acquired at 25 °C on a Bruker 500, 600, or 800 MHz spectrometer. The backbone ^{1}H, ^{13}C and ^{15}N resonances were assigned using standard three-dimensional triple-resonance HNCA, HN(CO)CA, HN(CA)CB and HN(COCA)CB experiments. The side-chain atoms were assigned from three-dimensional HCCH-TOCSY, HCCH-COSY and (H)C(CO)NH-TOCSY data. The NOE-derived distance restraints were obtained from ^{15}N- or ^{13}C-edited three-dimensional NOESY spectra. The $^{3}J(H^{N},H\alpha)$ coupling constants measured from three-dimensional HNHA data were used to determine ϕ-angle restraints. Slowly exchanging amide protons were identified from a series of two-dimensional ^{15}N-HSQC spectra recorded after $H_2O/^{2}H_2O$ buffer exchange. The intermolecular NOEs used in defining the structure of the Ago1 PAZ domain-UMP complex were detected in ^{13}C-edited (F_1), ^{13}C/^{15}N-filtered (F_3) three-dimensional NOESY spectra.

Structure calculations

Structures of the PAZ domain were calculated with a distance geometry simulated annealing protocol with X-PLOR[30]. Initial protein structure calculations were performed with manually assigned NOE-derived distance restraints. Hydrogen-bond distance restraints, generated from the H/D exchange data, were added at a later stage of structure calculations for residues with characteristic NOE patterns. The converged structures were used for the iterative automated NOE assignment by ARIA for refinement[31]. Structure quality was assessed with Procheck-NMR. The structure of the Ago1 PAZ domain–UMP complex was determined using the free-form structure in addition to 13 intermolecular NOE-derived distance restraints and four hydrogen-bond distance restraints.

RNA-binding assays

RNA and DNA oligonucleotide titration was performed by recording a series of two-dimensional ^{1}H-^{15}N-HSQC spectra with a uniformly ^{15}N-labelled PAZ domain (0.3 mM) in the presence of increasing amounts of RNA or DNA ranging from 0 to 0.9 mM. The protein sample and the RNA/DNA stock solutions were all prepared in the same buffer containing 100 mM sodium phosphate, 150 mM NaCl and 5 mM DTT-d_{10} at pH 6.5. Electrophoretic mobility shift assays were performed using a 26-nucleotide ssRNA (5′-AUUUUG-UUGUCGAAAAUUGUACAUAA-3′) labelled at the 5′ end using T4 polynucleotide kinase and [γ^{32}P]ATP. The protein/RNA samples were run on native TBE polyacrylamide gels and visualized by autoradiography. The concentration of the 5′ ^{32}P-labelled ssRNA was 2 μM in each EMSA experiment with a PAZ domain protein of

0–15 μM. For the competition EMSA, the corresponding unlabelled 26-nucleotide RNA or DNA of 0–30 μM was used in addition to the ^{32}P-labelled RNA and PAZ domain protein.

Site-directed mutagenesis

Expression constructs for mutant proteins were generated using the QuikChange site-directed mutagenesis kit (Stratagene). The presence of appropriate mutations was confirmed by DNA sequencing. Mutant proteins were purified by affinity chromatography using nickel-NTA columns (Qiagen). Proper folding of each PAZ domain mutant was confirmed by NMR. Samples for the NMR competition assay were prepared by mixing ^{15}N-labelled wild-type PAZ domain (0.2 mM), ssRNA oligonucleotide (5′-pUGACA) and unlabelled mutant PAZ domain with a molar ratio of 1:1:5.

Received 4 August; accepted 16 October 2003; doi:10.1038/nature02129.
Published online 16 November 2003.

1. Fire, A. *et al.* Potent and specific genetic interference by double-stranded RNA in *Caenorhabditis elegans*. *Nature* **391,** 806–811 (1998).
2. Dykxhoorn, D. M., Novina, C. D. & Sharp, P. A. Killing the messenger: short RNAs that silence gene expression. *Nature Rev. Mol. Cell Biol.* **4,** 457–467 (2003).
3. Hannon, G. J. RNA interference. *Nature* **418,** 244–251 (2002).
4. Hutvagner, G. *et al.* A cellular function for the RNA-interference enzyme Dicer in the maturation of the let-7 small temporal RNA. *Science* **293,** 834–838 (2001).
5. Grishok, A. *et al.* Genes and mechanisms related to RNA interference regulate expression of the small temporal RNAs that control *C. elegans* developmental timing. *Cell* **106,** 23–34 (2001).
6. Lee, R. C., Feinbaum, R. L. & Ambros, V. The *C. elegans* heterochronic gene lin-4 encodes small RNAs with antisense complementarity to lin-14. *Cell* **75,** 843–854 (1993).
7. Volpe, T. A. *et al.* Regulation of heterochromatic silencing and histone H3 lysine-9 methylation by RNAi. *Science* **297,** 1833–1837 (2002).
8. Hall, I. M. *et al.* Establishment and maintenance of a heterochromatin domain. *Science* **297,** 2232–2237 (2002).
9. Mochizuki, K., Fine, N. A., Fujisawa, T. & Gorovsky, M. A. Analysis of a piwi-related gene implicates small RNAs in genome rearrangement in tetrahymena. *Cell* **110,** 689–699 (2002).
10. Schramke, V. & Allshire, R. Hairpin RNAs and retrotransposon LTRs effect RNAi and chromatin-based gene silencing. *Science* **301,** 1069–1074 (2003).
11. Ratcliff, F., Harrison, B. D. & Baulcombe, D. C. A similarity between viral defense and gene silencing in plants. *Science* **276,** 1558–1560 (1997).
12. Waterhouse, P. M., Wang, M. B. & Lough, T. Gene silencing as an adaptive defence against viruses. *Nature* **411,** 834–842 (2001).
13. Zamore, P. D., Tuschl, T., Sharp, P. A. & Bartel, D. P. RNAi: double-stranded RNA directs the ATP-dependent cleavage of mRNA at 21 to 23 nucleotide intervals. *Cell* **101,** 25–33 (2000).
14. Bernstein, E., Caudy, A. A., Hammond, S. M. & Hannon, G. J. Role for a bidentate ribonuclease in the initiation step of RNA interference. *Nature* **409,** 363–366 (2001).
15. Knight, S. W. & Bass, B. L. A role for the RNase III enzyme DCR-1 in RNA interference and germ line development in *Caenorhabditis elegans*. *Science* **293,** 2269–2271 (2001).
16. Hammond, S. M., Bernstein, E., Beach, D. & Hannon, G. J. An RNA-directed nuclease mediates post-transcriptional gene silencing in *Drosophila* cells. *Nature* **404,** 293–296 (2000).
17. Hammond, S. M., Boettcher, S., Caudy, A. A., Kobayashi, R. & Hannon, G. J. Argonaute2, a link between genetic and biochemical analyses of RNAi. *Science* **293,** 1146–1150 (2001).
18. Tabara, H. *et al.* The rde-1 gene, RNA interference, and transposon silencing in *C. elegans*. *Cell* **99,** 123–132 (1999).
19. Williams, R. W. & Rubin, G. M. ARGONAUTE1 is required for efficient RNA interference in *Drosophila* embryos. *Proc. Natl Acad. Sci. USA* **99,** 6889–6894 (2002).
20. Cerutti, L., Mian, N. & Bateman, A. Domains in gene silencing and cell differentiation proteins: the novel PAZ domain and redefinition of the Piwi domain. *Trends Biochem. Sci.* **25,** 481–482 (2000).
21. Kambach, C. *et al.* Crystal structures of two Sm protein complexes and their implications for the assembly of the spliceosomal snRNPs. *Cell* **96,** 375–387 (1999).
22. Lau, N. C., Lim, L. P., Weinstein, E. G. & Bartel, D. P. An abundant class of tiny RNAs with probable regulatory roles in *Caenorhabditis elegans*. *Science* **294,** 858–862 (2001).
23. Reinhart, B. J. *et al.* The 21-nucleotide let-7 RNA regulates developmental timing in *Caenorhabditis elegans*. *Nature* **403,** 901–906 (2000).
24. Nykanen, A., Haley, B. & Zamore, P. D. ATP requirements and small interfering RNA structure in the RNA interference pathway. *Cell* **107,** 309–321 (2001).
25. Elbashir, S. M., Martinez, J., Patkaniowska, A., Lendeckel, W. & Tuschl, T. Functional anatomy of siRNAs for mediating efficient RNAi in *Drosophila melanogaster* embryo lysate. *EMBO J.* **20,** 6877–6888 (2001).
26. Schwarz, D. S., Hutvagner, G., Haley, B. & Zamore, P. D. Evidence that siRNAs function as guides, not primers, in the *Drosophila* and human RNAi pathways. *Mol. Cell* **10,** 537–548 (2002).
27. Martinez, J., Patkaniowska, A., Urlaub, H., Luhrmann, R. & Tuschl, T. Single-stranded antisense siRNAs guide target RNA cleavage in RNAi. *Cell* **110,** 563–574 (2002).
28. Lingel, A., Simon, B., Izaurralde, E. & Sattler, M. Structure and nucleic-acid binding of the *Drosophila* Argonaute 2 PAZ domain. *Nature* advance online publication, 16 November 2003 (doi:10.1038/nature02123).
29. Dostie, J., Mourelatos, Z., Yang, M., Sharma, A. & Dreyfuss, G. Numerous microRNPs in neuronal cells containing novel microRNAs. *RNA* **9,** 180–186 (2003).
30. Brunger, A. T. *X-PLOR Version 3.1: A System for X-Ray Crystallography and NMR* (Yale Univ. Press, New Haven, Connecticut, 1993).
31. Nilges, M. & O'Donoghue, S. Ambiguous NOEs and automated NOE assignment. *Prog. NMR Spectrosc.* **32,** 107–139 (1998).

Supplementary Information accompanies the paper on **www.nature.com/nature**.

Acknowledgements We thank R. W. Williams for providing a *D. melanogaster* Ago1 expressed sequenced tag clone, T. Tuschl for complementary DNAs encoding human Argonaute proteins, and T. A. Edwards for discussions. K.S.Y. is a recipient of a National Institutes of Health (NIH) predoctoral training grant fellowship. M.-M.Z. is supported by NIH grants, and is a member of the New York Structural Biology Center.

Competing interests statement The authors declare that they have no competing financial interests.

Correspondence and requests for materials should be addressed to M.-M.Z. (Ming-Ming.Zhou@mssm.edu). Coordinates for the NMR structure of the *D. melanogaster* Ago1 PAZ domain are deposited in the Protein Data Bank under ID code 1R4K.

addendum

Specific cytotoxic T cells eliminate cells producing neutralizing antibodies

Oliver Planz, Peter Seiler, Hans Hengartner & Rolf M. Zinkernagel

Nature **382,** 726–729 (1996).

The experiments in BALB/c mice using hybridoma technology reported in this Letter indicated that neutralizing-antibody-producing B cells and hybridomas could have been preferentially infected by lymphocytic choriomeningitis virus (LCMV), whereas B cells specific for the internal viral components were not. We concluded that during LCMV infection, B cells specific for the viral-surface antigens may be selectively and productively infected by LCMV through the membrane-anchored neutralizing-antibody receptor and are subsequently eliminated by virus-specific cytotoxic T lymphocytes. These experiments were performed in normal or $CD8^+$ T-cell-depleted BALB/c H-2^d mice. In later experiments designed to generalize these findings, we studied the infection patterns of hybridomas using C57BL/6 mice, but the results were variable and not conclusive. We also failed to observe a preferential infection of B cells or of hybridomas generated from IgM or isotype-switchable transgenic mice with a high percentage of neutralizing-antibody-expressing B cells[1,2]. In a third series of experiments with a recombinant virus that combines the envelope glycoprotein from vesicular stomatitis virus (VSV) with an LCMV replicon, we did not detect a preferential $CD8^+$ T-cell-dependent depletion of the anti-VSV antibody response (D. Pinschewer *et al.*, unpublished observations). We have also not so far been able to reproduce our original findings in new experiments with LCMV and BALB/c (SPF) mice. We therefore wish to alert the community to these problems until further experiments have been performed. □

1. Seiler, P. *et al.* Enhanced virus clearance by early inducible lymphocytic choriomeningitis virus-neutralizing antibodies in immunoglobulin-transgenic mice. *J. Virol.* **72,** 2253–2258 (1998).
2. Hangartner, L. *et al.* Antiviral immune responses in gene-targeted mice expressing the immunoglobulin heavy chain of virus-neutralizing antibodies. *Proc. Natl Acad. Sci. USA* **100,** 12883–12888 (2003).

